A novel benzodiazepine derivative that suppresses microtubule dynamics and impairs mitotic progression

Vittoria Pirani, Mathieu Métivier, Emmanuel Gallaud, Alexandre Thomas, Siou Ku, Denis Chrétien, Roberta Ettari, Régis Giet, Lorenzo Corsi, Christelle Benaud

A novel benzodiazepine derivative that suppresses microtubules dynamics and impairs mitotic progression

Vittoria Pirani[1,2], Mathieu Métivier[1], Emmanuel Gallaud[1], Alexandre Thomas[1], Siou Ku[1], Denis Chretien[1], Roberta Ettari[3], Regis Giet[1], Lorenzo Corsi[2*], Christelle Benaud[1 *]*

1- Univ Rennes, CNRS, IGDR (Institut de Génétique et Développement de Rennes) - UMR 6290, F-35000 Rennes, France
2- Dept. Life Sciences, University of Modena and Reggio Emilia, Modena, Italy
3- Dept. of Chemical, Biological, Pharmaceutical and Environmental Sciences, University of Messina, Messina, Italy

* Corresponding authors: christelle.benaud@univ-rennes1.fr, lorenzo.corsi@unimore.it, regis.giet@univ-rennes1.fr

Running title: A novel anti-mitotic benzodiazepine derivative

Key words: microtubules, mitosis, anti-mitotic drug, microtubule dynamics, SAC

Word number: 4046

Summary Statement: identification of a novel promising antimitotic drug with the unique properties altering microtubules growth and mitotic spindle organization.

Abstract

A novel 2,3-benzodiazepine-4 derivative, named 1*g*, has recently been shown to function as an anti-proliferative compound. We now show that it perturbs the formation of a functional mitotic spindle, inducing a spindle assembly checkpoint (SAC)-dependent arrest in human cells. Live analysis of individual microtubules indicates that 1*g* promotes a rapid and reversible reduction in microtubule growth. Unlike most anti-mitotic compounds, 1*g* does not interfere directly with tubulin, nor perturbs microtubules assembly *in vitro*. The observation that 1*g* also triggers a SAC-dependent mitotic delay associated with chromosome segregation in *Drosophila* neural stem cells, suggests it targets a conserved microtubules regulation module in human and flies. Altogether, our results indicate that 1*g* is a novel promising antimitotic drug with the unique properties altering microtubules growth and mitotic spindle organization.

Introduction

Microtubules are composed of α- and β-tubulin heterodimers whose assembly is highly dynamic, undergoing stochastic phases of growth and shrinkage, a process called dynamic instability (Mitchison and Kirschner, 1984). The microtubule network serves diverse and specific functions in differentiated cells such as scaffold and cargo transport. As the cell proceeds through mitosis, the microtubule network undergoes a dramatic reorganization to build a mitotic spindle used to equally segregate chromatids in the two daughter cells. *In vivo*, microtubules nucleation, organization as well as their intrinsic dynamic instability properties are regulated by microtubule-associated proteins (MAPS). The influence of MAPs on the dynamic assembly of microtubules contributes to the microtubules assembly patterns required for the proper formation of the mitotic spindle (Desai and Mitchison, 1997; Prosser and Pelletier, 2017).

The dynamic properties of mitotic spindle microtubules are required for fast and amphitelic attachment of sister kinetochores to the opposite spindle poles, an event essential to avoid missegregation of chromatids during anaphase and subsequent aneuploidy. In case of erroneous attachments of chromosomes to spindle microtubules, the spindle assembly checkpoint (SAC) remains unsatisfied and inhibits anaphase onset through inhibition of the Anaphase Promoting Complex/Cyclosome (APC/C). Cells are then delayed in mitosis until all defective attachments have been corrected (Khodjakov and Rieder, 2009).

The central role of microtubules in orchestrating cell division together with the property of SAC-dependent mitotic delay have made microtubules a target of choice for cancer chemotherapeutic agents aiming to block cell division (Janssen and Medema, 2011). Microtubules binding compounds that block microtubule dynamic, such as Vinka alkaloid and taxanes, have emerged as efficient anti-tumor agents and are currently used in therapeutic treatments. However, their use leads to severe side effects including neuropathy. Moreover, between tumors a variability in the response to the treatment with these compounds is observed. The identification of new anti-mitotic drugs with alternative modes of actions thus remains a priority for anti-cancer research (Dumontet and Jordan, 2010).

Activation of the AMPA receptor by glutamate has long been known to enhance cell proliferation (Stepulak et al., 2014). A recent screen to identify new anti-proliferative compounds has highlighted the non-competitive AMPA receptor agonist derivate 1-(4-amino-3, 5-dimethylphenyl)-3,5-dihydro-7,8-ethylenedioxy-4 h-2,3-benzodiazepin-4-one (called here after *1g)* as a potent novel growth inhibitor (Parenti et al., 2016). Upon treatment with 1*g*, human leukemia T cells accumulate with a 2N DNA content, suggesting an arrest of cells

at the G2/M phase of the cell cycle. In the current study, we have thus evaluated the potential of 1*g* as a novel promising and efficient anti-mitotic drug with a unique effect on microtubule growth.

Results

1g arrests cells in mitosis

A previous study has indicated that 1*g* induces an accumulation of Jurkat cells at the G2/M phase of the cell cycle (Parenti et al., 2016). To confirm the effect of 1*g* on the proliferation of transformed human epithelial cells, we followed an asynchronous population of Hela cells by phase contrast time-lapse microscopy for 20hrs (Fig. 1A; Movies S1 and S2). Control cells progressively rounded up to enter mitosis, divided and spread back down over this period of time, increasing the total number of cells. On the contrary, cells treated with 1*g* similarly rounded up, but no cell division was observed, suggesting that cells remained arrested in prometaphase and were unable to progress into anaphase and complete their division. This progressive accumulation of rounded cells was observable in a dose dependent manner with an optimal 1*g* concentration of 2.5µM (Fig. 1B,C).

To evaluate whether cells treated with 1*g* display a cell division defect, we synchronized Hela cells at the G2/M transition using the CDK1 kinase inhibitor RO3306 (Vassilev, 2006), then released them in presence of DMSO (control) or 1*g* and followed their progression through mitosis (Fig. 1D,E). Their mitotic stage was defined by staining the cells for tubulin and DNA. As expected, control cells reached the metaphase-anaphase transition within 45 min and 79% of the cells were in telophase at 90 min post-release. In contrast, only 6% of 1µM 1*g* treated cells had passed the metaphase-anaphase transition by 90 min and none of the dividing cells exposed to 2.5µM and 5µM 1*g* had reached anaphase. Furthermore, dividing cells treated with 2.5µM and 5µM 1*g* remained in prometaphase, displaying an abnormal mitotic spindle (Fig. 1D-lower right panel). Whereas control cells were able to fully congress their chromosomes to the metaphase plate within 45 min, cells treated with 1*g* still displayed major congression defects at 90 min (Figs 1D,F, 2B,D). This failure to establish a metaphase plate was associated with the detection of the SAC component BUBR1 on the kinetochore in agreement with an activation of the spindle assembly checkpoint (Fig. 1F). The drastic increase in the mitotic index (Fig.1C) of the asynchronous cell population after 16 hrs exposure to 1*g* implies that at high drug concentration, cells remain blocked in mitosis thru time (82±5 % in 2.5µM 1*g* vs 7.4 ±0.81 % in DMSO). Instead, the more modest increase in

mitotic index (26.8±0.8 % in 1μM 1*g* vs 82.0±5.0 % in 2.5μM 1*g*) when cells are exposed to 1μM 1*g* suggests that at suboptimal 1*g* concentrations, cells can progress through mitosis but with extensive delay. Indeed, anaphase figures could be observed 4 hrs post-released in cells treated with 1μM 1*g,* but not with higher concentrations (data not shown).

To confirm that the accumulation of rounded cells observed in the asynchronous cell population treated with 1*g* (Fig. 1A) was indeed due to the activation of the SAC making the cells unable to exit mitosis, HeLa cells were treated with 1*g* alone or in combination with the SAC inhibitor AZ3146 (Tipton et al., 2013), and followed by videomicroscopy. In presence of AZ3146, 1*g* treated cells progressively rounded up, but unlike cells treated with 1*g* alone, proceeded through a defective anaphase-telophase and spread back down. It is interesting to note that these cells displayed no cytosolic sign of cell death throughout the 16hrs of the treatment with both inhibitors (Fig. 1G and Movies S3 and S4). This data indicate that 1*g* impacts cell proliferation via mitotic arrest and not direct cell death. However, prolong mitotic arrest has been shown to result in subsequent cell death (Brito and Rieder, 2006; Stanton et al., 2011) explaining the previously described apoptotic effect of the 1*g* compound observed after 48hrs of treatment (Parenti et al., 2016). All together these experiments demonstrate that treatment of proliferating Hela cells with 1*g* activates the SAC, arresting the cells in prometaphase.

***1g* disrupts the formation of the mitotic spindle**

The disorganized mitotic spindle observed in 1*g* treated cells, prompted us to further characterize the dynamics of the mitotic spindle assembly. To that purpose, we imaged by spinning microscopy live HeLa cells expressing GFP-tubulin after their release from the CDK1 inhibitor induced G2/M arrest (Fig. 2A,B movies S5, S6 and S7). Control cells treated with DMSO rapidly separated their spindle poles and 100% of the cells formed a bipolar spindle within 15±4 min (Fig. 2C). All cells achieved full chromosome congression into a metaphase plate and progressed into anaphase in an average time of 55±7 min (Fig. 2B,D). When treated with low 1*g* concentrations (1μM), 90% of the cells formed a bipolar spindle within 28±13 min. However, at 80 min post NEB, 90% of 1μM treated cells still displayed unaligned chromosomes and thus had not satisfied the SAC (arrow head fig 2B). At higher 1*g* concentrations (2.5-5μM), several microtubule nucleation sites could be observed and the microtubule growth from centrosomes was strongly reduced (Fig. 2A -arrow heads). Albeit clustering of the microtubule asters could be observed, in 70% of the cells exposed to 2.5μM

1*g* and in 100% of those treated with 5μM, 3 asters or more were present and strong chromosome congression defects were observed at 80min post NEB (Fig. 2B arrows, D, E). No bipolar mitotic spindles were formed at those concentrations (Fig. 2C). Visualization of the centrosomes, using Hela cells expressing the centriolar protein centrin-GFP, confirmed that microtubule nucleation emanated from the two centrosomes. However, the additional small asters observed did not contain centrin-GFP, indicating that 1*g* did not trigger centrosome amplification (Fig. 2G). In addition, a decrease of 25% (1μM 1*g*) and 37% (2μM 1*g*) in spindle poles distance compared to control cells was observed (Fig. 2F). The defect in centrosome separation was further accentuated at 5μM, with 64% decrease in distance between centrosomes in cells treated with 5μM 1*g* as compared to DMSO (Fig. 2H). The formation of shorter microtubules observed in presence of 1*g* most likely accounts for the reduced centrosome separation, since centrosome separation is a microtubule dependent process occurring in prophase and prometaphase (Wittmann et al., 2001).

***1g* alters microtubule growth in cells**

The dynamic properties of microtubules are crucial for the extensive remodeling of interphase arrays of microtubules into a mitotic bipolar spindle (Desai and Mitchison, 1997). We thus investigated whether 1*g* interferes with microtubule polymerization. We first performed a depolymerization-repolymerization type of assay (Fig. 3A). The microtubule network of interphase cells was depolymerized at 4°C in presence or absence of 1*g*. We then followed the dynamics of microtubules regrowth as the samples were returned to 37°C. Long newly nucleated microtubules could be observed 5 min after the temperature switch in control cells, and extensive microtubule repolymerization was present after 10 min. Presence of 1*g* did not affect cold induced depolymerization of microtubules, indicating that 1*g* does not act as a microtubule stabilizing agent (Fig. 3A t=0 and G). Indeed, in presence of stabilizing agents, such as taxan, cold resistant microtubules bundles can be detected (Stanton et al., 2011). However, 1*g* markedly slowed down the dynamics of the microtubule network reformation (Fig 3A t=5,10 and 15min). Only short and fragmented microtubules were observed in 1*g* treated cells in the first 10 min, and it required 30 min to polymerize a microtubule network equivalent to the one formed after 15 min in control cells.

The growing microtubule +tip protein EB1 has been commonly used to image microtubule + ends and to quantify their dynamics (Matov et al., 2010). To further investigate and quantify the effect of 1*g* on microtubule dynamics, we imaged HeLa cells expressing EB1-

GFP by spinning disk confocal microscopy at 1 sec time intervals before and immediately after addition of *1g* or DMSO (Fig. 3B and movies S8, S9). In control Hela cells, measurements of EB1 comets velocity indicated a microtubules growth speed of 16.6 ±0.83 µm.min-^{1}. Whereas addition of DMSO in control cells did not significantly alter microtubule growth speed, 1*g* treatment resulted in 25% decrease in mean growth rate (from 14.2±0.3 before to 10.6±0.3 µm.min-^{1} 1*g* 2.5µM) (Fig. 3C,D) without affecting the median growth lifetime. Furthermore, the initial microtubule growth pattern (before treatment, Fig. 3B,C) was recovered shortly after drug removal (washout, Fig. 3B,C) indicating that the action of 1*g* is reversible (15.3 ±1.1 µm.min-^{1}after washout)(Fig. 3B,C, panels and Movies S8, S9). 1*g* treatment did not significantly alter the number of nucleation events (Fig. 3E), nor the number or duration of growth pauses (Fig. 3F). In control cells, we could infer a shrinkage rate of 32.9±2.2 µm.min^{-1}, which was not statistically different in DMSO treated cells (34.5±1.7 µm.min^{-1}). In presence of 1*g*, no shrinkage events were detected. When tracking EB1 comets shrinkage can only be inferred when followed by significant EB1 labelled microtubule regrowth (Matov et al., 2010). The absence of detectable shrinkages in presence of 1*g* could be explained by the fact that the main events occurring were terminal shortenings and shrinkage followed by short or slow growth phases that did not produce detectable EB1-comets within the temporal window analyzed. We thus clearly observed a slowdown in microtubules polymerization in interphase cells. Altogether, these data indicate that 1*g* is able to promote a fast and reversible inhibition of microtubules growth during interphase and mitosis.

To assess whether the *1g* compound targets directly tubulin polymerization, we tested the impact of *1g* on microtubule self-assembly *in vitro*. We performed turbidity assays classically used to analyze the effect of drugs or MAPs on microtubule assembly, including microtubule nucleation and elongation (Gallaud et al., 2014)(Fig. 3G). Absorbance at 350 nm, which is directly proportional to the amount of microtubule polymers formed, revealed no significant difference when purified tubulin was incubated in polymerizing buffer at 37° C in presence of a range of 1*g* concentrations or DMSO. More specifically, we did not observe any effect of the drug on nucleation (same lag-phases at different concentrations), on elongation (sigmoid) phase, nor on the plateau of polymerization (total mass of microtubules assembled). In addition, no significant formation of aggregates was detected when the temperature was shifted back to 0°C, the average absorbance going back to the base line for all samples. The

absence of significant alteration in tubulin polymer assembly, or on formation of aggregates indicates that 1*g* does not interfere with microtubule self-assembly directly.

1g interferes with cell division in tissue

During the last decades, *Drosophila Melanogaster* has emerged as an interesting model to identify new genes required for cell division as well as for cancer research (Gonzalez, 2013). Therefore, we have examined the impact of the compound on neural stem cells (neuroblasts) division, in the developing brain of *Drosophila* larvae. Third instar larval brain expressing RFP-α-tubulin and H2A-GFP were dissected and cultured in Schneider medium containing DMSO, or various concentrations of 1*g*. For comparison, we used in parallel 20µM Taxol and 10µM Nocodazole treatments (Fig. 4A, S1). Control neuroblasts formed bipolar spindles and started to segregate their chromosomes 5.9±0.4 min after the nuclear envelope breakdown (NEB). As expected, following prolonged mitotic arrest, neuroblasts treated with Taxol or Nocodazole underwent slippage (Fig. S1D,E). In presence of 1*g,* mitosis duration was significantly increased in a dose-dependent manner (6.1±0.6 min, 8.2±0.6 min and 10.9±3.1 min for 5µM, 10µM and 20µM treatment respectively) (Fig 4D), suggesting an activation of the SAC. The delay observed was in the range of the one observed in Msps-depleted neuroblasts (15.5±0.8 min, *n*=44) (Fig. S1D), a MAP whose down regulation has been described to severely disrupt the integrity of the mitotic spindle (Cullen et al., 1999). Furthermore, in agreement with SAC activation, 1*g* treated neuroblasts exhibited dose-dependent mitotic spindle–assembly defects (5µM: 35,3%, 10µM: 100% of neuroblasts) (Fig. 4B). Lagging chromatids were frequently observed in 31,3% (n=6/17) and 68,4 % (n=13/19) of the neuroblasts treated respectively with 10 and 20µM of 1*g* (Fig. 4C). In 79% (n=42) of the cells, we observed the presence of tripolar spindles and the formation of two central spindles (Fig. 4A, 1*g* 8,9,13min, Fig. 4E,F). The outcome of mitosis was variable. Whereas some cells proceed to double cytokineses leading to the formation of three daughter cells (Fig.4A, 1*g*-dotted lines 13min), in some instances, regression of the initial double cytokinesis furrow could also be observed. In either case, following defective division 1*g* treated neuroblast progenies were able to polymerize microtubules from their interphase centrosome (Fig. 4G,H).

Discussion

We here show that the anti-proliferative effect of 1*g* in cancer cell lines observed previously (Parenti et al., 2016) is caused by interference with microtubule polymerization and defective mitotic spindle assembly, leading consequently to SAC activation. Noteworthily, the 1*g* concentrations used in cell treatments (5µM or less) are 20 times inferior to the Kd for the AMPA receptor (Kd>100 µM (Micale et al., 2008)), indicating that the strong effects of 1*g* on cell division are independent of the AMPA receptor signaling pathway.

Our *in vitro* assays with pure tubulin indicate that 1*g* does not directly target the intrinsic microtubule polymerization. When used *in cellulo* or *in vivo*, we did not observe the massive effects on the microtubule cytoskeleton that are triggered with microtubule binding agents such as taxol or nocodazole. Instead, under 1*g* treatment, the overall architecture of HeLa cells interphase microtubules network remains intact. Moreover, *Drosophila* neuroblasts are still able to nucleate *de novo* microtubules from the daughter centrosome following division. As cells proceed from interphase to mitosis a 10 fold increase in the turnover rate of microtubules is required for the reorganization of the microtubule network into a mitotic spindle and for the capture of chromosomes (Desai and Mitchison, 1997; Prosser and Pelletier, 2017). This change in microtubule turnover rate implies that a drug that moderately impedes microtubule dynamics in interphase is expected to trigger more drastic effects on mitotic microtubules. Indeed, the main effect of 1*g* was observed during cell division in fly brain neuroblasts and in HeLa cells.

In both systems exposed to 1*g*, SAC activation is observed resulting either in a mitotic delay in fly neuroblasts or mitotic arrest in mammalian cells. While neuroblasts treated with taxol or nocodazole that severely impairs spindle assembly remained arrested and underwent mitotic slippage, the mitotic delay in fly neuroblasts treated with 1*g*, did not exceed 3 times the duration of cell division. The presence of kinetochores unattached by the microtubules of the mitotic spindle is responsible for SAC activation and mitotic arrest. In 1*g* treated neuroblast, the observation of a mitotic delay rather than a mitotic arrest, suggests that albeit displaying a tripolar shape the spindle microtubules still manage to grow and correctly attach kinetochores. However, the altered microtubule growth result in a time delay to perform that task and satisfy the SAC. On the other hand, HeLa cells remained arrested following 1*g* treatment. The difference in genome size could account for this difference in 1*g* drug response. Fly cells harbors only four chromosomes making it easier to achieve kinetochore attachment under defective MT polymerization and thus satisfy the SAC and exit mitosis. By

contrast, SAC satisfaction is likely more problematic for HeLa cells which requires the correct attachment of 70-82 chromosomes (Landry et al., 2013).

Nevertheless, the mitotic phenotypes are similar between neuroblasts and HeLa cells: the centrosomal microtubule asters are present, but they only nucleate short microtubules. Moreover, additional microtubule asters are detected, that fails to coalesce into a bipolar structure. This inability to form a bipolar spindle suggests that not only the growth of MT is altered but also the structure of the metaphase spindle, such as the organization/bundling of the interpolar microtubules. Altogether our results support the hypothesis that 1*g* targets a MAP involved in the regulation of microtubule growth during interphase and mitosis and which is essential for mitotic spindle assembly. The similarities in the mitotic phenotypes observed in Hela cells and fly neural stem cells indicate that the 1*g* target and its functional motifs are likely conserved between human and flies. Further studies will be needed to identify the direct cellular target of 1*g* in order to obtain further insight on its mechanism of action.

Microtubules targeting agents are wildly used in chemotherapy, but their lack of specificity for dividing tumor cells is a limitation. Indeed, their toxicity for the neural, immunological and gastric systems, due to their profound effect on interphase microtubules functions as well as tumor resistance, foster a need for development of new agents (Dumontet and Jordan, 2010; Stanton et al., 2011). Target of choice are cellular microtubules regulators that modulates microtubule dynamics and organization specifically in proliferating cells. As discussed above the 1*g* compound may comply with the requirement of new pharmaceuticals compounds with a more specific mode of action.

Materials and methods

Cell Culture

HeLa Kyoto cells were grown in Dulbecco's modified Eagle's medium Glutamax (Gibco) supplemented with 10% fetal calf serum (PAA), 100U/ml penicillin and 100ug/ml streptomycin. For synchronization experiments, cells were treated for 16 hrs with 5µM RO-3306 to arrest cells in G2/M, cells were then washed in complete medium and released for the indicated times.

pEGFP-Tub (BD bioscience), pGFP- EB1 (gift from P. Chavrier, Institut Curie, Fr) and were used respectively to generate, Tubulin-GFP and EB1-GFP HeLa stable cell line.

Small Molecules Inhibitors

1*g* was synthesized by R. Ettari (University of Messina, Italy) (Parenti et al., 2016) and its purity verified by 1H NMR and 13C NMR. Absence of contaminants was also subsequently confirmed by HPLS-MS-MS. 1g was dissolved in DMSO at a stock concentration of 50 mM. Further dilutions were performed in tissue culture medium. DMSO control treatment is equivalent to the amount of DMSO present in the highest 1*g* treatment concentration used in the experiment. The final DMSO concentrations in the assays were therefore inferior or equal to 0.01% in Hela cell experiments and 0.04% for drosophila tissue experiments.
Mps1 inhibitor AZ3146 was from Calbiochem, the CDK1 inhibitor RO-3306 from Merck, Taxol and Nocodazol from Sigma Aldrich.

Antibodies, Immunoblotting and Immunofluorescence

The following commercial antibodies were used: α-tubulin (clone YL1/2, Millipore; 1:1000), anti-BUBRI (clone 9, BD bioscience; 1:500), anti-GFP (clone7.1and13.1, Roche; 1:1000), anti-Phospho Histone H3 (clone CMA312, Millipore; 1:1000). DNA was stained with Hoechst 33342 or To-Pro-3 iodide (Invitrogen). For microtubule immunofluorescence staining, cells were grown on glass coverslips and fixed with methanol at -20°C (tubulin). For BubR1 staining, cells were first permeabilized with 0,5 % Triton in PHEM (60mM PIPES, 25 mM HEPES, 10 mM EGTA, 4mM $MgSO_4.7H_2O$) for 5 minutes at room temperature and then fixed with PFA in PHEM for 10 minutes. Antibody staining was then performed as described previously (Benaud et al., 2004). Brain from wandering third instar larvae were dissected and maintained in 100 µl of Schneider media supplemented with DMSO or 20 µM 1*g* for 1 h at 25°C before fixation and immunostaining as described previously (Gallaud et al., 2014).

Drosophila stocks

Flies were maintained under standard conditions at 25°C. w^{1118} flies were used as controls for immunostaining experiments. Flies expressing H2A-GFP (Clarkson and Saint, 1999) and the recombinant Insc-Gal4, UAS-Cherry-α-tubulin as well as the flies *UAS-ChRFP::Tubulin* (BDSC 25774) and *Insc-Gal4* (BDSC 8751) were obtained from the Bloomington Drosophila Stock Center (Indiana University, #5941 and #25773 respectively). The flies expressing ubiquitously Tubulin tagged with RFP (RFP-tub) is a gift from Renata Basto (Institut Curie, Paris, France). The cell membrane marker (Ubi-PH(PLCγ)-GFP (Gervais et al., 2008) is a gift from Antoine Guichet (Institut Jaccques Monod, Paris, France). The Msps RNAi line (ref. GD21982) was purchased from the Vienna Drosophila RNAi Center. The knock down of *Msps* in central brain neuroblasts was driven by Insc-Gal4.

Live Cell Imaging and Microscopy

For live imaging, *Drosophila* brains expressing H2A-GFP and Cherry-α-tubulin were dissected in Schneider's *Drosophila* medium containing 10% FCS. Following 10 min pre-incubation with DMSO or the indicated concentration of chemical compounds, isolated brains were loaded and mounted on stainless steel slides. The preparations were sealed with mineral oil (Sigma) as previously described (Gallaud et al., 2014). Hela cells were grown in Lab-Tek I chambered cover-glasses (Nunc). Bright field images of asynchronous dividing Hela cells were acquired every 5 min with a 20x objective on a DMRIBE inverted microscope (Leica) equipped with CO_2 heated incubator chamber and a CoolSNAP ES BW camera (Roper scientific). Live fluorescent images were acquired on a spinning disk microscope using a Plan Apo 60x/1,4 NA objective on an Eclipse Ti-E microscope (Nikon) equipped with a spinning disk (CSU-X1; Yokogawa), a thermostatic chamber (Life Imaging Service), Z Piezo stage (Marzhauser), and a charge-coupled device camera (CoolSNAP HQ2; Roper Scientific). Drosophila live images were alternatively acquired with a spinning disk system consisting of a DMi8 microscope (Leica) equipped with a 63X/1.4NA oil objective, a CSU-X1 spinning disk unit (Yokogawa) and an Evolve EMCCD camera (Photometrics). The microscope is controlled by the Inscoper Imaging Suite and the dedicated software (Inscoper).

For Hela cells, time-lapse Tubulin-GFP images were acquired every 1min for the 45min time lapse or every 5min for the 90min time lapse, and EB1GFP comets every 0.5sec using Metamorph Software (Universal imaging). For drosophila neuroblasts, Z-series were acquired every 30 or 60 seconds. Immunofluorescence images of fixed samples were acquired with SP5 confocal microscope (Leica), or with an API DeltaVision microscope equipped with a coolSnapHQ camera (Princeton instruments) using the SoftWorX software. Image acquisition was coupled to deconvolution when indicated. Images were processed and measurements performed using Fiji software (*http://fiji.sc/*). Analysis of EB1comets were performed using the Matlab based open source u-track particle tracking (version2.0) software (Danuser Lab, UT Southwern Medical Center).

Turbidimetry assay

Commercial lyophilised tubulin (PurSolutions, Nashville, USA) was reconstituted at 500 µM in distilled water according to the manufacturer instructions. Tubulin was diluted at 50 µM in 10 % glycerol, 1 mM GTP, 0.02 % DMSO in BRB80 buffer (80 mM K-Pipes, 1 mM EGTA, 1mM $MgCl_2$, pH 6.8 with KOH), and in the presence of 0 µM, 5 µM or 10 µM *1g*. Control samples contained the same amount of DMSO as *1g* samples. Suspensions were centrifuged

at 33,000 g at 4 °C for 5 min before polymerisation. Samples were transferred into 100 µl quartz cuvettes (Hellma), and measurements at 350 nm were performed in a UVIKON XS spectrophotometer thermostated at 35 °C to stimulate tubulin polymerisation. After 30 min of polymerisation, depolymerisation was induced by a cold temperature shift at 4 °C to assess the presence of aggregates.

Acknowledgement

The imaging work was performed on the platform MRic-Photonics (BIOSIT, Université Rennes1). We thank Thibault Courtheoux for his help with the use of plus Tip Tracker software and Laurent Richard-Parpaillon for critical discussion.

Conflict of interest

The content of this manuscript is included in a current patent application

Funding

VP was financed by Erasmus+ program. CB is supported by INSERM and La Ligue Régionale Contre le Cancer (Grand Ouest-Bretagne), DC by the French National Agency for Research (ANR-16-CE11-0017-01), LC by Fondazione di Vignola 2014, RE by FFABR_RU2017 MIUR, MM and AT by La Ligue Régionale Contre le Cancer (Grand Ouest-Bretagne), Region Bretagne, EG by La foundation pour la Recherche Medicale (DEQ20170336742) and RG by La Ligue and ARC. This work was supported by the CNRS, the University of Rennes 1.

References

Benaud, C., Gentil, B. J., Assard, N., Court, M., Garin, J., Delphin, C. and Baudier, J. (2004). AHNAK interaction with the annexin 2/S100A10 complex regulates cell membrane cytoarchitecture. *J Cell Biol* **164**, 133–144.

Brito, D. A. and Rieder, C. L. (2006). Mitotic checkpoint slippage in humans occurs via cyclin B destruction in the presence of an active checkpoint. *Curr Biol* **16**, 1194–1200.

Clarkson, M. and Saint, R. (1999). A His2AvDGFP fusion gene complements a lethal His2AvD mutant allele and provides an in vivo marker for Drosophila chromosome behavior. *DNA Cell Biol* **18**, 457–462.

Cullen, C. F., Deak, P., Glover, D. M. and Ohkura, H. (1999). mini spindles: A gene encoding a conserved microtubule-associated protein required for the integrity of the mitotic spindle in Drosophila. *J Cell Biol* **146**, 1005–1018.

Desai, A. and Mitchison, T. J. (1997). Microtubule polymerization dynamics. *Annu Rev Cell Dev Biol* **13**, 83–117.

Dumontet, C. and Jordan, M. A. (2010). Microtubule-binding agents: a dynamic field of cancer therapeutics. *Nat Rev Drug Discov* **9**, 790–803.

Gallaud, E., Caous, R., Pascal, A., Bazile, F., Gagne, J.-P., Huet, S., Poirier, G. G., Chretien, D., Richard-Parpaillon, L. and Giet, R. (2014). Ensconsin/Map7 promotes microtubule growth and centrosome separation in Drosophila neural stem cells. *J Cell Biol* **204**, 1111–1121.

Gervais, L., Claret, S., Januschke, J., Roth, S. and Guichet, A. (2008). PIP5K-dependent production of PIP2 sustains microtubule organization to establish polarized transport in the Drosophila oocyte. *Development* **135**, 3829–3838.

Gonzalez, C. (2013). Drosophila melanogaster: a model and a tool to investigate malignancy and identify new therapeutics. *Nat Rev Cancer* **13**, 172–183.

Janssen, A. and Medema, R. H. (2011). Mitosis as an anti-cancer target. *Oncogene* **30**, 2799–2809.

Khodjakov, A. and Rieder, C. L. (2009). The nature of cell-cycle checkpoints: facts and fallacies. *J Biol* **8**, 88.

Landry, J. J. M., Pyl, P. T., Rausch, T., Zichner, T., Tekkedil, M. M., Stutz, A. M., Jauch, A., Aiyar, R. S., Pau, G., Delhomme, N., et al. (2013). The genomic and transcriptomic landscape of a HeLa cell line. *G3 (Bethesda)* **3**, 1213–1224.

Matov, A., Applegate, K., Kumar, P., Thoma, C., Krek, W., Danuser, G. and Wittmann, T. (2010). Analysis of microtubule dynamic instability using a plus-end growth marker. *Nat Methods* **7**, 761–768.

Micale, N., Colleoni, S., Postorino, G., Pellicano, A., Zappala, M., Lazzaro, J., Diana, V., Cagnotto, A., Mennini, T. and Grasso, S. (2008). Structure-activity study of 2,3-benzodiazepin-4-ones noncompetitive AMPAR antagonists: identification of the 1-(4-amino-3-methylphenyl)-3,5-dihydro-7,8-ethylenedioxy-4H-2,3-benzodiazepin-4-o ne as neuroprotective agent. *Bioorg Med Chem* **16**, 2200–2211.

Mitchison, T. and Kirschner, M. (1984). Dynamic instability of microtubule growth. *Nature* **312**, 237–242.

Parenti, S., Casagrande, G., Montanari, M., Espahbodinia, M., Ettari, R., Grande, A. and Corsi, L. (2016). A novel 2,3-benzodiazepine-4-one derivative AMPA antagonist inhibits G2/M transition and induces apoptosis in human leukemia Jurkat T cell line. *Life Sci* **152**, 117–125.

Prosser, S. L. and Pelletier, L. (2017). Mitotic spindle assembly in animal cells: a fine balancing act. *Nat Rev Mol Cell Biol* **18**, 187–201.

Stanton, R. A., Gernert, K. M., Nettles, J. H. and Aneja, R. (2011). Drugs that target dynamic microtubules: a new molecular perspective. *Med Res Rev* **31**, 443–481.

Stepulak, A., Rola, R., Polberg, K. and Ikonomidou, C. (2014). Glutamate and its receptors in cancer. *J Neural Transm (Vienna)* **121**, 933–944.

Tipton, A. R., Ji, W., Sturt-Gillespie, B., Bekier, M. E. 2., Wang, K., Taylor, W. R. and Liu, S.-T. (2013). Monopolar spindle 1 (MPS1) kinase promotes production of closed MAD2 (C-MAD2) conformer and assembly of the mitotic checkpoint complex. *J Biol Chem* **288**, 35149–35158.

Vassilev, L. T. (2006). Cell cycle synchronization at the G2/M phase border by reversible inhibition of CDK1. *Cell Cycle* **5**, 2555–2556.

Wittmann, T., Hyman, A. and Desai, A. (2001). The spindle: a dynamic assembly of microtubules and motors. *Nat Cell Biol* **3**, E28–34.

Figure Legends

Figure 1: 1*g* arrests proliferating cells in prometaphase and activates the spindle assembly checkpoint. A- Proliferation of HeLa cells treated with DMSO or 1*g* (5µM) monitored by imaging asynchronous cells for 16 and 20hrs. scale bar=30µm (full sequence in Movies S1 and S2). **B-** Dose response effect of 1*g* on cell proliferation. Phase contrast images of HeLa cells treated with the indicated concentration of 1*g* for 16hrs. scale bar=30µm. **C-** Mitotic index (% mitotic cells/total cells) of HeLa cells treated with DMSO or the indicated concentration of 1*g* for 16hrs (n≥150 cells). Student t-test, ****P<0.0001. **D-**Cells synchronized at the G2-M transition were released in presence of DMSO or the indicated concentration of 1*g* for 45min (metaphase in control cells) or 90min (telophase in control). Cells are stained for α–tubulin in green and DNA in magenta. scale bar=10µm. **E-** Quantification of mitotic cells repartition in the different phases of mitosis in presence of increasing concentration of 1*g* (n≥80 cells). **F-** HeLa cells synchronized at the G2/M transition were released in presence of DMSO or 5µM 1*g* for 45 min. Z stack projections of cells stained for the presence at the kinetochore of the SAC protein BUBR1 and DNA. scale bar=5µm. **G-** Activation of the SAC arrests 1*g* treated cells in prometaphase. Live phase contrast imaging of proliferating asynchronous HeLa cells treated with 5µM 1*g* alone or in combination with 2µM AZ3146. scale bar=30µm. (full sequence in Movies S3 and S4).

Figure 2: 1*g* interferes with mitotic spindle assembly in dividing cells. A-Spinning disk images (Max projection) of HeLa tubulin-GFP cells undergoing mitosis in presence of DMSO, 1µM or 2,5µM 1*g*. Scale bar=10µm. (full sequence in Movies S5, S6 and S7). **B-** HeLa expressing tubulin-GFP (green) and H2B-mcherry (red) imaged for 90min following G2/M released in presence of DMSO or the indicated concentration of 1*g*. t0= nuclear envelop breakdown (NEB); Arrows points to microtubule asters and arrow head to unaligned chromosomes. Scale bar=10µm. **C-**Quantification of % cells treated with the indicated concentration of 1*g* forming a bipolar spindle by 80 min. n≥15. **D-** Quantification of % cells congressing their chromosomes into a metaphase plate by 80 min. n≥15. **E-** Quantification of the number of microtubules asters in cells treated with the indicated concentration of 1*g* at t=80min. n≥18. **F-**Analysis of the distance between spindle poles, 45 min after the G2/M block release in cells treated with DMSO or 1µM and 2µM of 1*g*. n≥40 cells. **G-** HeLa centrin-GFP cells synchronized at the G2/M transition were released for 45 min in presence of DMSO or 5µM 1*g* and stained for tubulin, GFP and DNA. DeltaVision deconvoluted

projections, scale bar=5µm. **H-** Analysis of centrosome separation in cells treated with DMSO or 5µM 1*g*. n≥49 cells. Student t-test, ****P<0.0001.

Figure 3: 1*g* alters microtubules growth in cells. A-Microtubules of HeLa cells treated with DMSO or 5µM 1*g* were depolymerized at 4°C (t0) and allowed to repolymerize by switching back the cells to 37°C for the indicated times. Z stack projection images of cells stained for α–tubulin. **B-** Spinning disk time lapse images of HeLa EB1-GFP cells (1 image/sec) before treatment, in presence of DMSO or 2,5µM 1*g*, and after washing out the drug (control: Movie S8; 1*g*: Movie S9). Time projection of EB1-GFP over 1 min are presented for the different conditions. C-Kymograph (time (sec) vs distance) representations of the EB1 tracks over 1 min. Scale bar=1µm. Quantification of EB1 comets velocity (**D-**) nucleation events (**E-**) and inferred number of pauses (**F-**). For each condition n≥700 tracks in 10 (control) to 15 (1*g*) independent measurements. ****P<.0001, Student's t-test. **G-** *In vitro* microtubule polymerization assay. DMSO (ctl) or 5 and 10 µM 1*g* was added to purified tubulin in polymerization buffer at 4°C. The formation of microtubule polymers was monitored by the absorbance at 350nm as the temperature was increased to 35°C. Formation of stable aggregates are visualized as temperature is shifted back to 4°C.

Figure 4: Effect of 1*g* on *Drosophila* neuroblasts proliferation.
Dividing neural stem cells of drosophila brains expressing tubulin-RFP and Histone H2B-GFP imaged by spinning disk confocal microscopy. **A-** Selected frames of dividing *Drosophila* larval neuroblasts incubated with DMSO or 1*g*. Time 00:00 (min:sec) = NEB. Dotted circle outlines the neuroblast cell contour (t5-t9) and the neuroblast progeny (t12): neuroblast (large dotted circle) and ganglion mother cell GMC (small dotted circle). Scale bar: 10µm. **B-**Analysis of the percentage of mitotic spindle assembly defects in neuroblasts treated with DMSO or 1*g*. n≥17 cells for each condition. **C-** Analysis of chromosomes segregation defects corresponding to lagging chromosomes in DMSO and 1*g* treated brains. n≥17 cells. **D-** Analysis of mitosis duration measured from NEB to anaphase onset in neuroblasts exposed to DMSO (05:87±0.1, *n*=43), 5µM (06:14±0.19, *n*=17), 10µM (08:24±0.19, n=17), 20µM (10:60±0.5, *n*=42) 1*g*. **P<0.0012; ***P<$1.3x10^{-4}$ (Wilcoxon test). **E-** Analysis of the frequency of formation of tripolar spindle in neuroblast treated with DMSO (0%, *n*=44) or 20µM 1*g* (87%, *n*=42). **F-** Z stack image of prometaphase neuroblasts incubated for 1hr in DMSO or 1*g* and stained for α–tubulin (green) and DNA

(magenta). Arrow heads points to tripolar asters. scale bar=10μm. **G,H-** Selected frames illustrating interphase aster reformation following mitosis of *Drosophila* larval neuroblasts incubated with DMSO or 1*g*. Arrow points to interphase aster. Scale bar=10μm.

Figure1

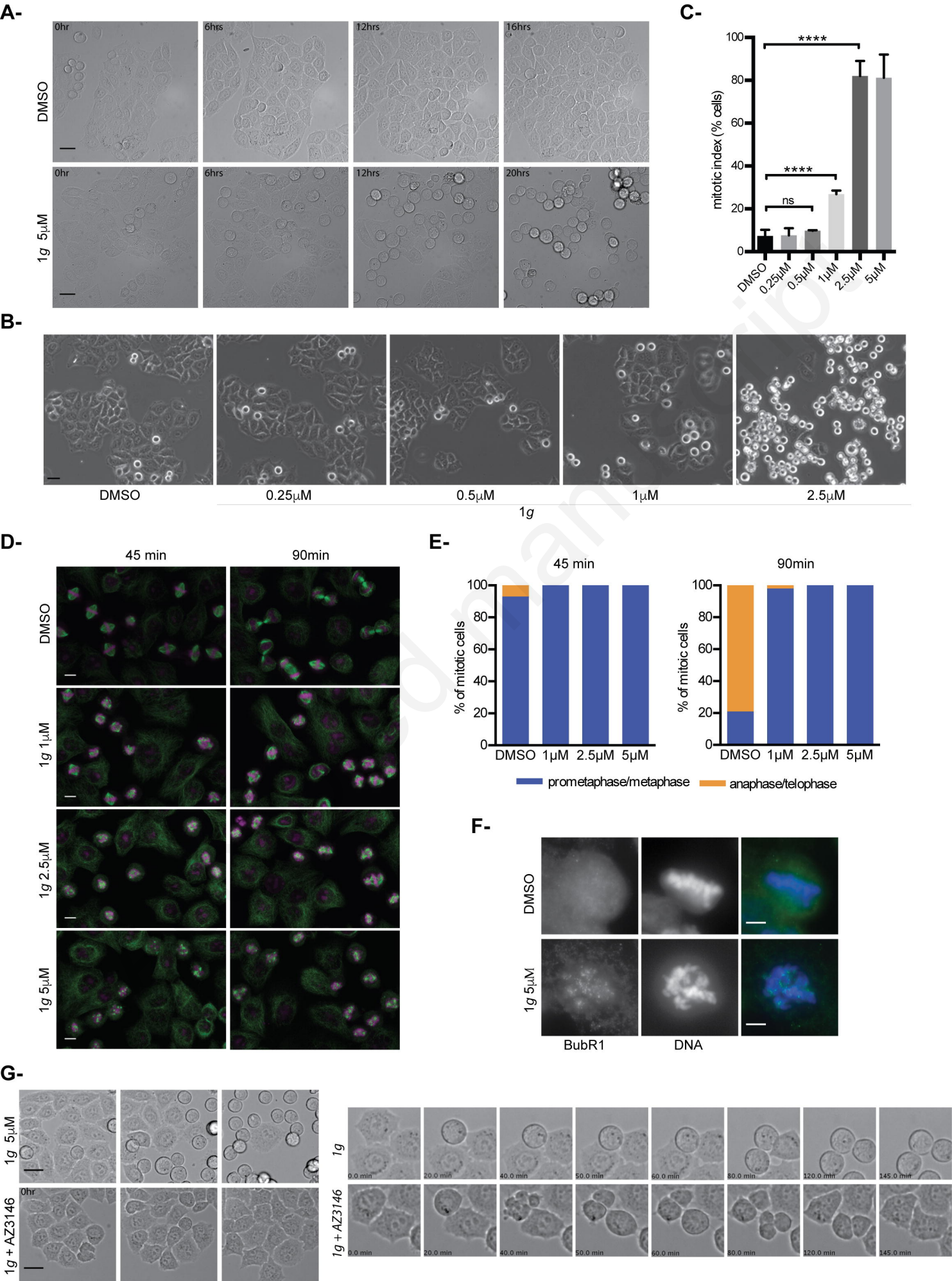
A-
0hr
6hrs
12hrs
16hrs
DMSO
0hr
6hrs
12hrs
20hrs
1g 5μM
C-
mitotic index (% cells)
100
80
60
40
20
0
****
****
ns
DMSO
0.25μM
0.5μM
1μM
2.5μM
5μM
B-
DMSO
0.25μM
0.5μM
1μM
2.5μM
1g
D-
45 min
90min
DMSO
1g 1μM
1g 2.5μM
1g 5μM
E-
45 min
90min
% of mitotic cells
100
80
60
40
20
0
DMSO 1μM 2.5μM 5μM
prometaphase/metaphase
anaphase/telophase
F-
DMSO
1g 5μM
BubR1
DNA
G-
1g 5μM
0hr
1g + AZ3146
1g
1g + AZ3146
0.0 min
20.0 min
40.0 min
50.0 min
60.0 min
80.0 min
120.0 min
145.0 min

Figure 2

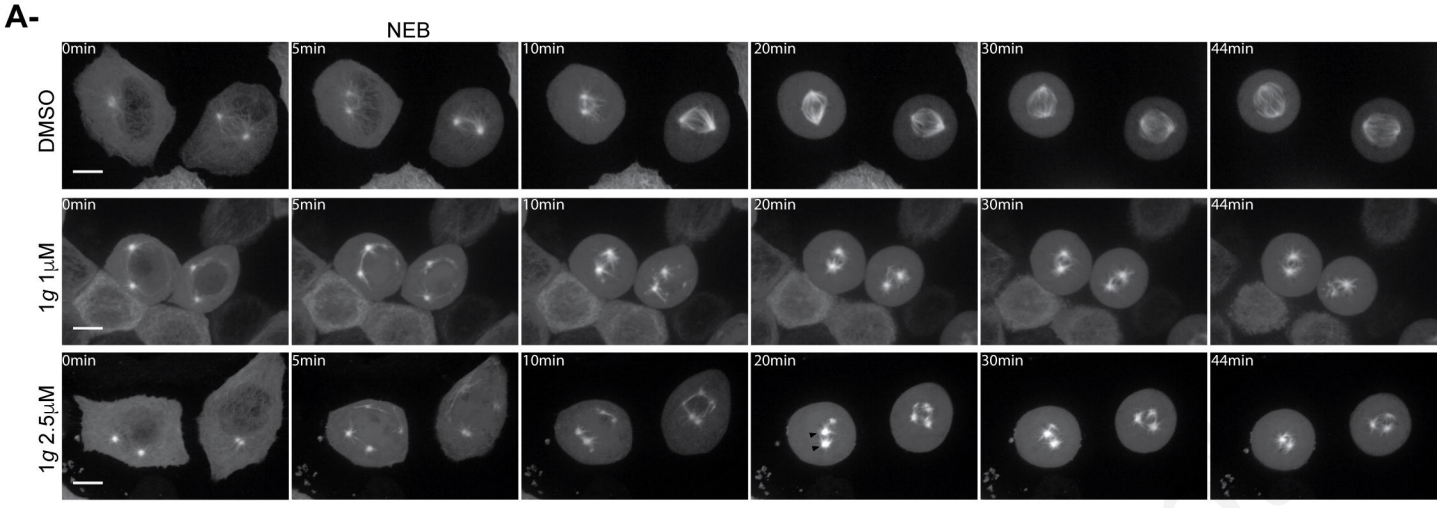

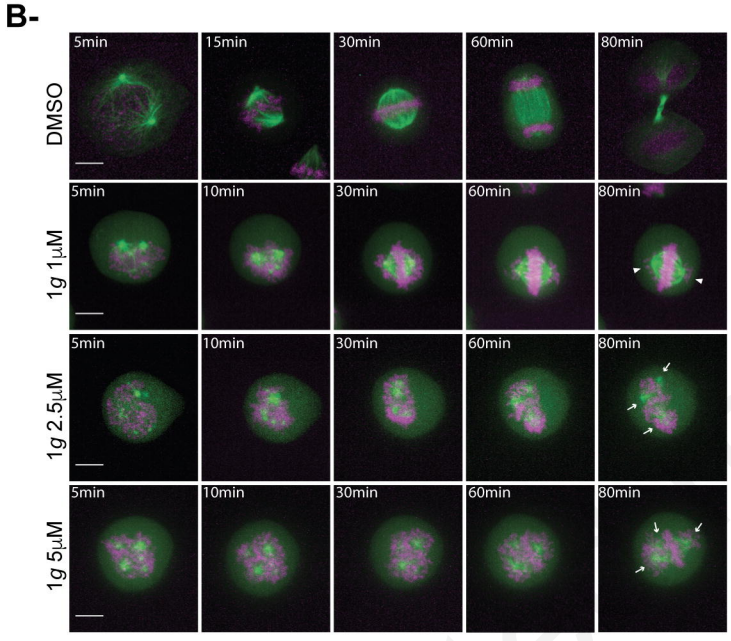

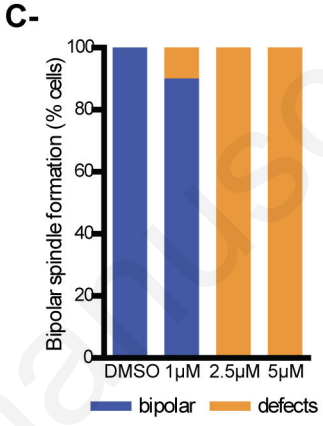

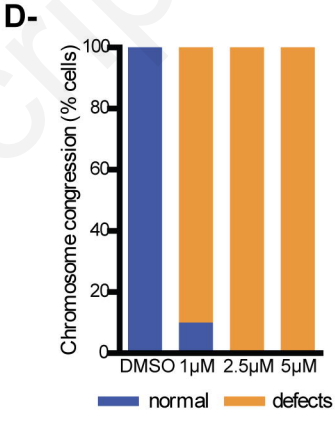

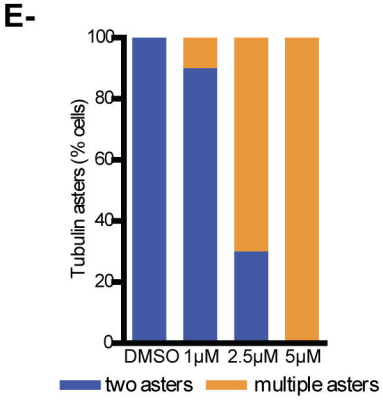

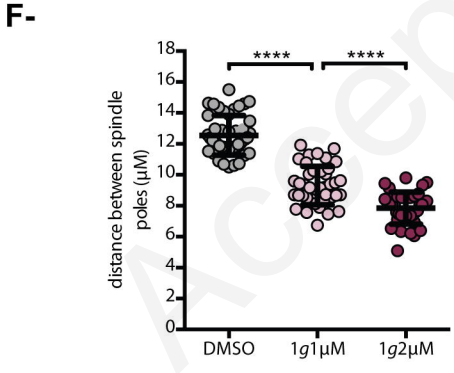

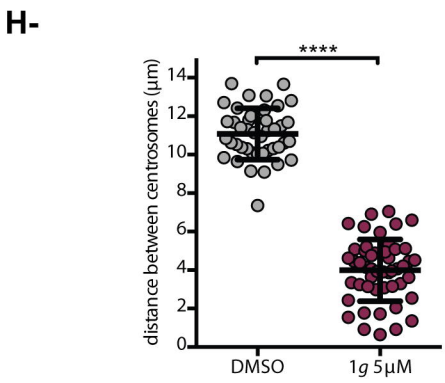

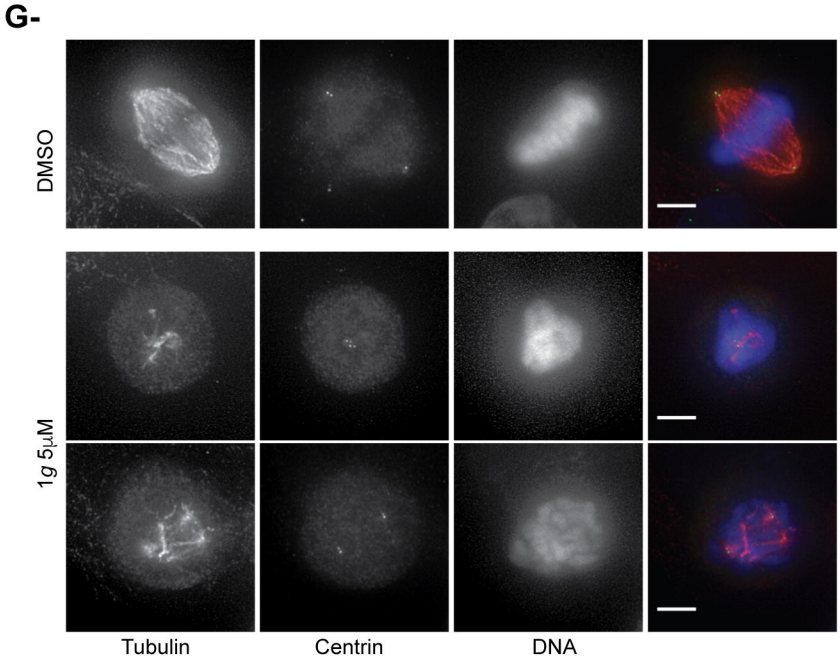

Figure 3

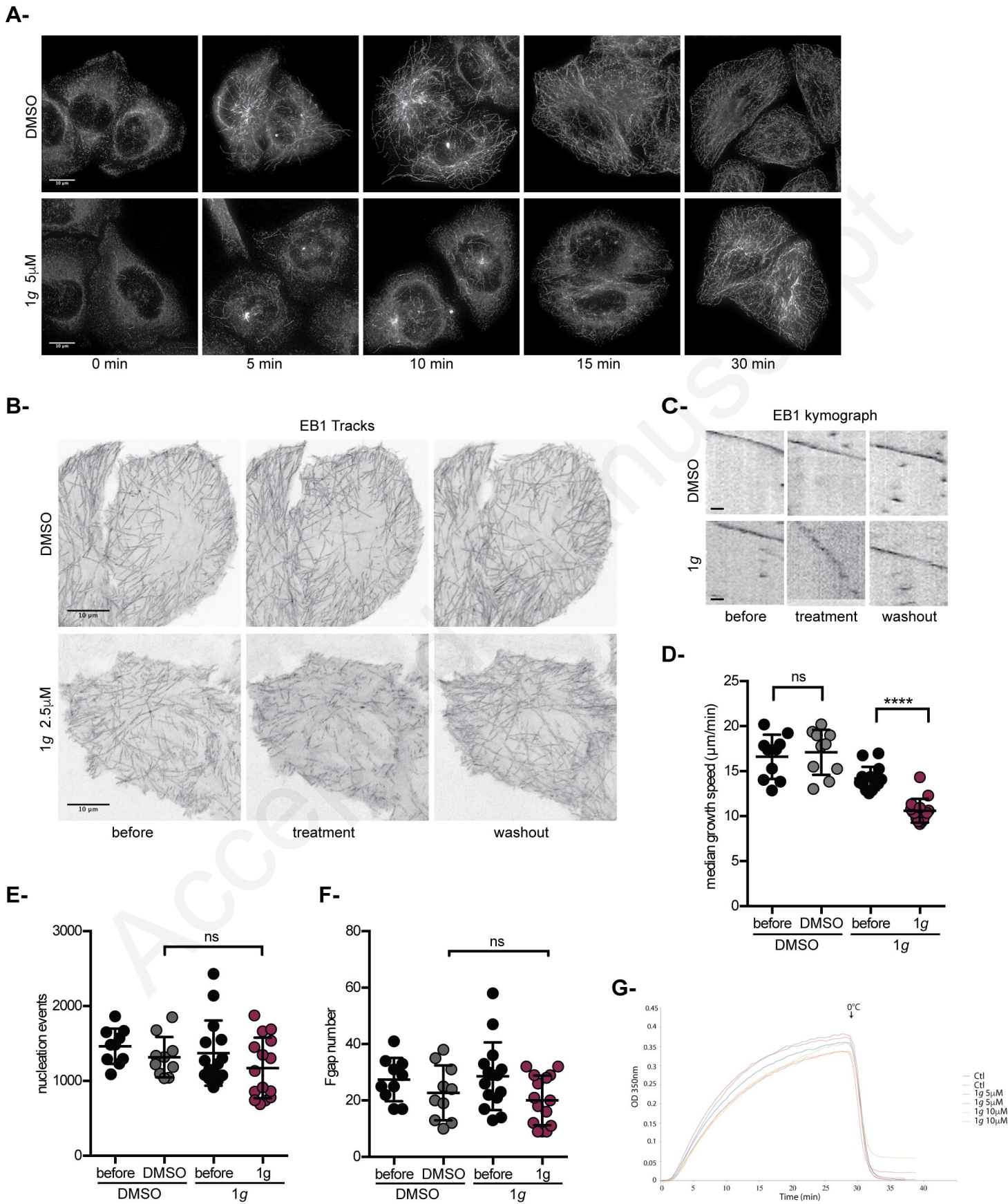
A-
DMSO
1g 5µM
0 min
5 min
10 min
15 min
30 min
B-
EB1 Tracks
DMSO
1g 2.5µM
before
treatment
washout
C-
EB1 kymograph
DMSO
1g
before
treatment
washout
D-
median growth speed (µm/min)
ns
****
before
DMSO
before
1g
DMSO
1g
E-
nucleation events
ns
before
DMSO
before
1g
DMSO
1g
F-
Fgap number
ns
before
DMSO
before
1g
DMSO
1g
G-
OD 350nm
0°C
Time (min)
Ctl
Ctl
1g 5µM
1g 5µM
1g 10µM
1g 10µM

Figure 4

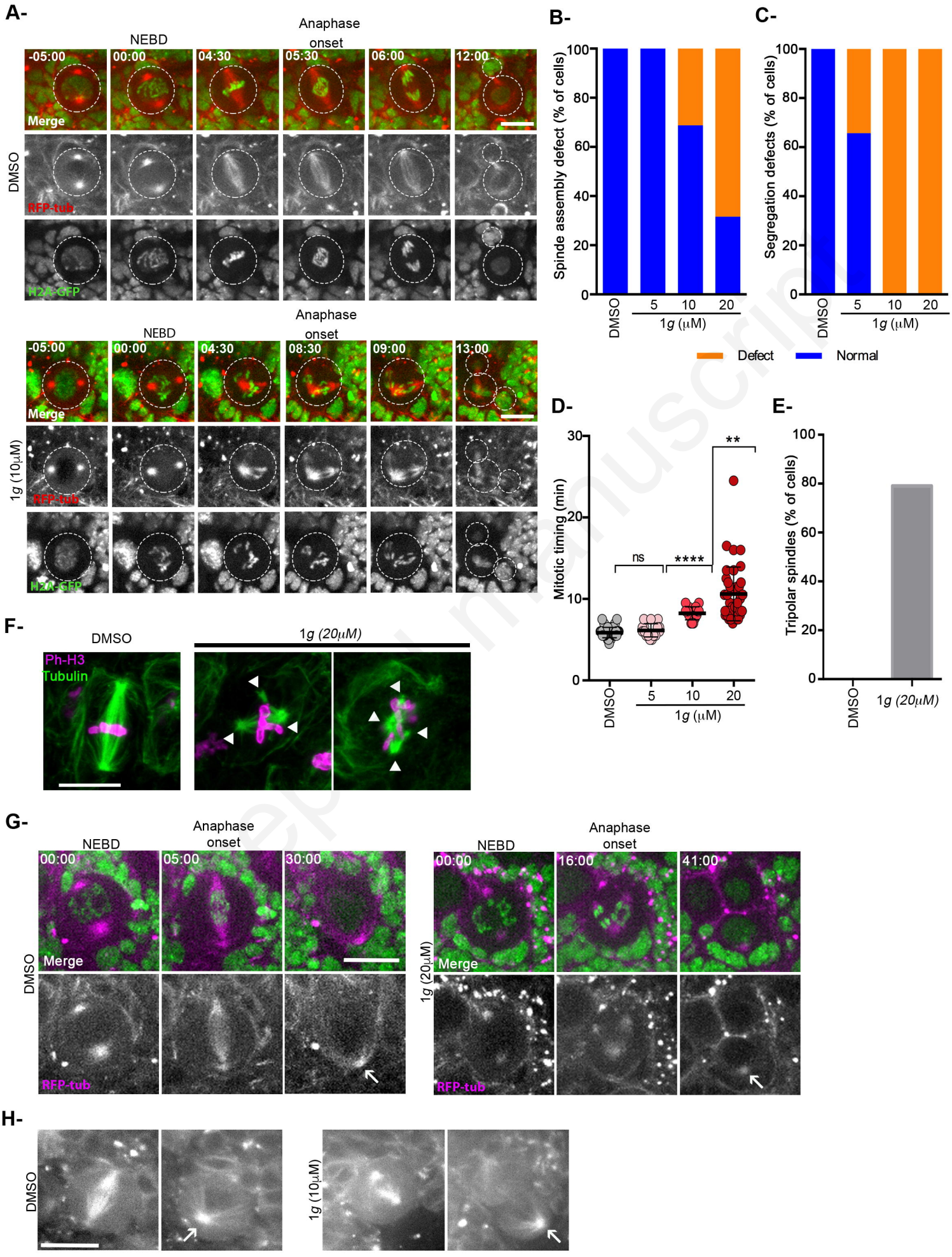
A-
NEBD
Anaphase onset
-05:00
00:00
04:30
05:30
06:00
12:00
Merge
DMSO
RFP-tub
H2A-GFP
08:30
09:00
13:00
1g (10μM)
B-
Spinde assembly defect (% of cells)
C-
Segregation defects (% of cells)
DMSO
5
10
20
1g (μM)
Defect
Normal
D-
Mitotic timing (min)
ns
****
**
E-
Tripolar spindles (% of cells)
1g (20μM)
F-
Ph-H3
Tubulin
G-
16:00
41:00
H-